





# IR-820@NBs Combined with MG-132 Enhances the Anti-Hepatocellular Carcinoma Effect of Sonodynamic Therapy

Xiaodong Wang , Chunyue Wang , Huimin Tian , Yichi Chen, Bolin Wu, Wen Cheng 

Department of Ultrasound, Harbin Medical University Cancer Hospital, Harbin, People's Republic of China

Correspondence: Wen Cheng; Bolin Wu, Department of Ultrasound, Harbin Medical University Cancer Hospital, No. 150, Haping Road, Nangang District, Harbin, 150081, People's Republic of China, Tel +86 13313677182; +86 15663615088, Email [chengwen@hrbmu.edu.cn](mailto:chengwen@hrbmu.edu.cn); [wubolin@hrbmu.edu.cn](mailto:wubolin@hrbmu.edu.cn)

**Purpose:** Sonodynamic therapy (SDT) is a promising and significant measure for the treatment of tumors. However, the internal situation of hepatocellular carcinoma (HCC) is complex, separate SDT treatment is difficult to play a good therapeutic effect. Here, we used SDT combined with MG-132 to mediate apoptosis and autophagy of HCC cells to achieve the purpose of treatment of cancer.

**Methods:** To determine the generated reactive oxygen species (ROS) and the change of mitochondrial membrane potential ( $\Delta\Psi_m$ ), HepG2 cells were stained by 2,7-dichlorodihydrofluorescein diacetate (DCFH-DA) and 5,5',6,6'-Tetrachloro-1,1',3,3'-tetraethylimidacarbocyanine iodide (JC-1) staining to determine the IR-820@NBs-mediated SDT to achieve HCC therapy through the mitochondrial pathway. Cell counting kit 8 (CCK-8) assay and flow cytometry were used to detect cell viability and apoptosis rate of HepG2 cells. Autophagy was detected by mCherry-GFP-LC3B fluorescence labeling. Chloroquine (Cq) pretreatment was used to explore the relationship between autophagy and apoptosis. To detect the ability of HepG2 cells migration and invasion, cell scratch assay and transwell assay were used.

**Results:** The successfully prepared IR-820@NBs could effectively overcome the shortcomings of IR-820 and induce lethal levels of ROS by ultrasound irradiation. As a dual agonist of apoptosis and autophagy, MG-132 could effectively enhance the efficacy of SDT in the process of treating HCC. After pre-treatment with Cq, the cell activity increased and the level of apoptosis decreased, which proved that apoptosis and autophagy were induced by combined therapy, autophagy, and apoptosis have the synergistic anti-tumor effect, and part of apoptosis was autophagy-dependent. After combined therapy, the activity and invasive ability of HCC cells decreased significantly.

**Conclusion:** SDT combined with MG-132 in the process of treating liver cancer could effectively induce apoptosis and autophagy anti-tumor therapy, which is helpful to the research of new methods to treat liver cancer.

**Keywords:** sonodynamic therapy, MG-132, apoptosis, autophagy, hepatocellular carcinoma

## Introduction

Liver cancer is the sixth most familiar tumor in the world and the fourth leading cause of cancer-related death.<sup>1</sup> Hepatocellular carcinoma (HCC) is the main type of liver cancer, and nearly 85% of patients with liver cancer represent HCC.<sup>2</sup> At present, the main treatment methods of HCC include surgery, TACE, radiofrequency ablation, and systemic anti-tumor therapy. However, due to the limitations of these treatments, tumor recurrence, and chemotherapy resistance, the median five-year survival rate of patients with HCC is below 20%.<sup>3</sup> Therefore, it is urgent to find a new treatment to increase the overall survival rate of patients with HCC. Sonodynamic therapy (SDT) is a new therapeutic method developed based on photodynamic therapy (PDT). Compared with other treatments, SDT has gradually stepped into the public view because of its non-invasive and higher safety. At the same time, the penetrating power of ultrasound (US) is stronger than that of light, and SDT is more suitable for adjuvant therapy or alternative therapy for deep organ tumors.<sup>4</sup>

SDT mediates tumor cell death by inducing intracellular production of reactive oxygen (ROS) by low-frequency US irradiation with sonosensitizers.<sup>5</sup> The type and function of sonosensitizer determine the therapeutic effect of SDT.

Traditional sonosensitizers such as hematoporphyrin and near-infrared (NIR) dyes are mainly derived from photosensitizers.<sup>6,7</sup> New indocyanine green (IR-820), derived from NIR dye ICG, has stronger stability, circulation ability, and ROS induction ability in vivo.<sup>8</sup> However, the poor dispersion and strong hydrophobicity limited the use of IR-820 in the therapy process.<sup>9</sup> Nanocarriers, including nanobubbles (NBs), are used to solve these problems. NBs are composed of phospholipid bilayers encapsulating inert gases, which show positive stability and passive tumor targeting ability (based on enhanced permeability and retention effect, EPR effect), and can be used to load drugs.<sup>10</sup> The combined application of ultrasound-targeted nanobubble destruction (UTND) technology and NBs can achieve the targeted release of drugs and improve the drug uptake rate of cancer cells.<sup>11,12</sup> Therefore, loading IR-820 on NBs can not only overcome the shortcomings of IR-820 but also increase the drug uptake rate of tumor cells. At the same time, IR-820 can be a sonosensitizer to mediate SDT and induce the production of lethal degrees of ROS in HCC cells, thus realizing the SDT therapy of HCC.

The role of apoptosis (type I programmed cell death) and autophagy (type II programmed death) in the occurrence and growth of cancer are important.<sup>13</sup> The occurrence of apoptosis is mainly mediated by the death receptor pathway (external pathway) and the mitochondrial pathway (internal pathway).<sup>14</sup> All external and internal apoptosis pathways lead to the activation of the caspase protease family.<sup>15</sup> The accumulation of intracellular ROS will cause mitochondrial damage, and change the permeability of the mitochondrial outer membrane. And then, cytochrome C (Cyt C) is released, which will cause the caspase cascade reaction and induce cell apoptosis.<sup>16</sup> Due to the influence of extrinsic and intrinsic factors, apoptosis is one of the main death modes of tumor cells.<sup>17</sup> Autophagy is a regulated process that exists in cell growth, including the formation of autophagosomes enclosing cytoplasm and transporting them to lysosomes for degradation.<sup>18</sup> The effect of autophagy in cancer cells is opposite in the process of tumor growth. On the one hand, low-level autophagy can help cancer resist the environmental pressure caused by excessive growth and the pressure caused by treatment, and achieve the role of promoting tumor growth.<sup>19,20</sup> On the other hand, excessive autophagy can inhibit cancer directly or by promoting other ways of cell death, such as apoptosis and ferroptosis.<sup>21–23</sup> SDT mainly cure tumor by inducing tumor cell apoptosis, but autophagy also exists in the process of treatment.<sup>24</sup> Therefore, apoptosis combined with autophagy-mediated tumor therapy can be regarded as one of the directions of SDT in subsequent research.

Ubiquitin-proteasome system (UPS) and autophagy are the main intracellular protein degradation pathway. Intracellular short-lived proteins are mainly degraded by UPS, while autophagy mainly degrades long-lived proteins.<sup>25</sup> Intracellular apoptosis signals are degraded mainly by UPS.<sup>26</sup> 26S proteasome is the main proteasome in cells and the key to UPS. Cbz-leu-leu-leucinal (MG-132) is a reversible 26S proteasome inhibitor, which can effectively inhibit UPS.<sup>27</sup> The treatment of tumors with MG-132 can inhibit the degradation of tumor cell apoptosis signal, thus promoting tumor cell apoptosis. At the same time, autophagy can be activated responsively due to the inhibition of UPS.<sup>28</sup> Therefore, MG-132 can be used as a dual agonist of apoptosis and autophagy.

In this study, we used IR-820 as a sonosensitizer to mediate SDT in HCC therapy. The advantages of IR-820 could achieve the effect of SDT better in the treatment of HCC. The construction of IR-820@NBs could effectively overcome the shortcomings of IR-820 and reduced the toxicity to normal cells. The particle size of IR-820@NBs realized the targeted drug delivery and release of sonosensitizer by EPR effect and UTND technology. Due to the complex growth mechanism of HCC, separate SDT treatment could not achieve the purpose of treatment well. SDT exerts anti-tumor effect mainly by mediating tumor cells apoptosis. However, a certain degree of autophagy will reduce the therapeutic effect of SDT. Therefore, we choose the combination of SDT and MG-132, a dual agonists of apoptosis and autophagy, to induce apoptosis and autophagy of HCC cells to achieve apoptosis combined with autophagy synergistic anti-tumor therapy.

## Materials and Methods

### Fabrication and Characterization of IR-820@NBs

To compose IR-820@NBs, we dissolved 1,2-distearoyl-sn-glycero-3-phosphocholine (DSPC, MedChemExpress, USA), 1,2-distearoyl-sn-glycero-3-phosphoethanolamine-mPEG-2000 (DSPE-MPEG2000, MedChemExpress, USA) and IR-820 in a mixture made up of chloroform and methyl alcohol which at a volumic ratio of 2: 1. The molar ratio of DSPC, DSPE-MPEG2000, and IR-820 (MedChemExpress, USA) was 90: 10: 1. And then, the organic solvent in the

mixture were evaporated in a water bath at the temperature of 60 °C. Next, 5mL preheated phosphate-buffered saline (PBS, Procell, Wuhan, China) and the dried phospholipid mixture were subsequently hydrated in a sealed tube at the temperature of 60 °C. The particle size of IR-820@NBs was uniform by phospholipid extrusion technology. After that, replace the air in the tube with perfluoropropane ( $C_3F_8$ ; Research Institute of Physical and Chemical Engineering of Nuclear Industry, Tianjin, China) with a syringe. Finally, the tube was mechanically vibrated for 60s at a frequency of 60 Hz, using a mechanical oscillator (YJT Medical Apparatuses and Instruments, Shanghai, China). The mixed liquid was placed at 4 °C for 20 min and was centrifuged for 3 min at 600 rpm. Subsequently, the liquid clarified in the lower layer is extracted. The final IR-820@NBs were mixed with PBS uniformly for further analysis (Figure 1A).

The morphology of IR-820@NBs was observed by transmission electron microscopy (TEM, Hitachi TEM system, Japan). Then, we determined the hydrodynamic diameter, zeta potential, and polydispersity index (PDI) by dynamic light scattering (DLS) using a particle size analyzer (Nano-2s ZEN3600, Malvern Panalytical Limited, UK). The absorption spectrum was recorded by a DU-640 ultraviolet-visible spectrophotometer (Beckman Coulter Inc., Brea, CA) to determine that IR-820 was carried on NBs successfully and count the drug incorporation efficiency of IR-820@NBs. To further assess the stability of IR-820@NBs, they were stored at 37 °C for 24 h and then observed by TEM.

## Cell Culture

HepG2 cells, the human HCC cell line, was derived from the Institute of Cancer Research affiliated with Harbin Medical University, and sanctioned by the Ethics Committee of Harbin Medical University. The HepG2 cells were cultivated in Dulbecco's Modified Eagle Medium (DMEM, Gibco, Carlsbad, CA) with 10% fetal bovine serum (FBS, PAN, Germany) and 0.01% mycoplasma removal agent (Beyotime Institute of Biotechnology, Jiangsu, China) in the humidified incubator containing 5% carbon dioxide at 37 °C.

## Experimental Grouping

As shown in Table 1, group A is a blank control group, and the cells were not treated. The HepG2 cells in group B were treated with IR-820 and irradiated by US (frequency: 1 MHz, power density: 3 W/cm<sup>2</sup>, duty cycle: 50%, Institute of Ultrasound Imaging, Second Affiliated Hospital of Chongqing Medical University, Chongqing, China) with specific parameters. In group C, cells were treated with MG-132 (MedChemExpress, USA) alone. Group D and Group E were

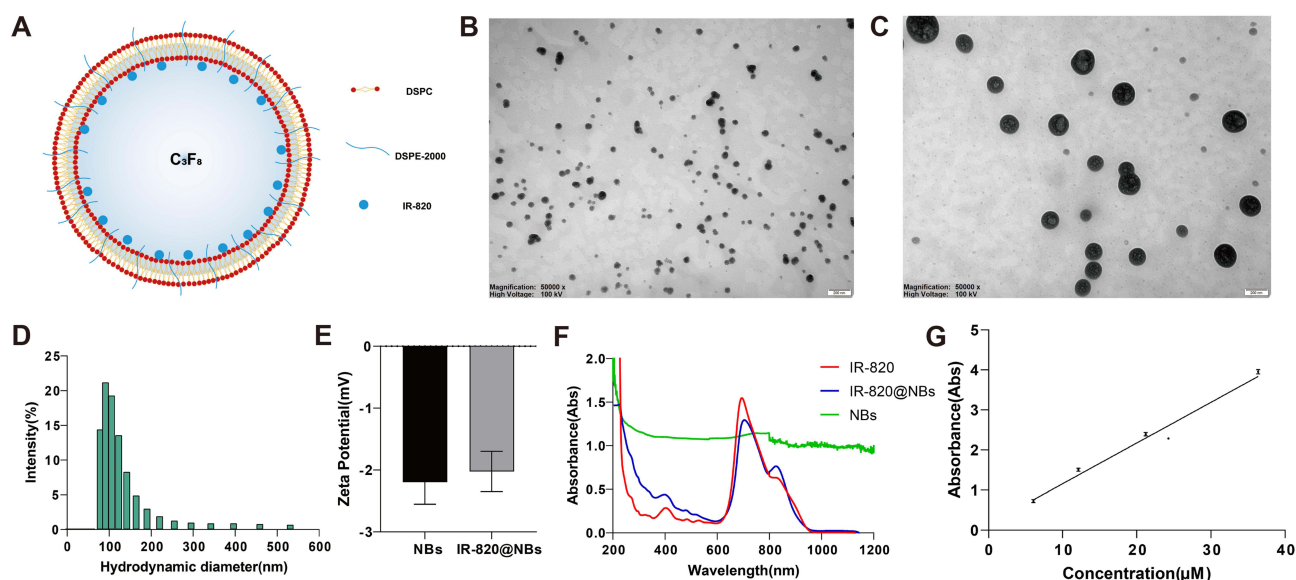


**Figure 1** Preparation and Characterization of the IR-820@NBs. (A) The microstructural schematic representation of IR-820@NBs. (B) Transmission electron microscopy (TEM) image of IR-820@NBs at 0 h. (C) TEM image of the IR-820@NBs stored at 37 °C for 24 h. (D) Hydrodynamic diameter of IR-820@NBs measured by DLS. (E) Zeta potential of IR-820@NBs and pure NBs. (F) Absorption spectra of IR-820@NBs, IR-820, and NBs. (G) The concentration absorption intensity curve of IR-820.

**Table 1** HepG2 Cells Were Treated with Different Treatment Methods

Experimental Group	Treatment Methods
Group A	NC
Group B	IR-820+US
Group C	MG-132
Group D	IR-820+MG-132
Group E	IR-820@NBs+MG-132
Group F	IR-820@NBs+MG-132+US
Group G	IR-820@NBs+MG-132+US+Cq

treated with IR-820 or IR-820@NBs combined with MG-132 without using US. Group F was treated with SDT combined with MG-132. In group G, cells were treated with chloroquine(Cq) to inhibit the occurrence of autophagy.

## Cytotoxicity Assay

About  $5 \times 10^3$  HepG2 cells per well were cultured in 96-well-microplates for 24 h. And then, the fresh DMEM compounding different concentrations of IR-820, MG-132, or the mixed liquid of IR-820@NBs and MG-132 would be substituted for old DMEM. After 40 min of treatment, cells incubated with IR-820 or IR-820@NBs were irradiated with US for 60s. Cell counting kit 8 (CCK-8) assay was used to assay the viability of HepG2 cells after 24 h of drug treatment. Based on the instructions, 100  $\mu$ L of CCK-8 solution (Abbkine Inc., Wuhan, China) including 90  $\mu$ L fresh DMEM without FBS were added to each well. The absorption value of each well was measured by microplate reader (Multiskan FC, Thermo Fisher Scientific, USA) at a wavelength of 450 nm after being cultured for 45 min at 37 °C in the dark.

## Detection of Intracellular ROS Generation

The level of ROS generative in HepG2 cells was examined by using 2,7-dichlorodihydrofluorescein diacetate (DCFH-DA, Abbkine Inc., Wuhan, China). About  $5 \times 10^5$  HepG2 cells per well were cultured in 6-well-microplates for 24 h and then provided different treatments. After US irradiation for 30 min, DCFH-DA at a final concentration of 10  $\mu$ M was loaded in per well for 30 min at 37 °C in the dark. Subsequently, each well was washed with PBS three times, and the fluorescence intensity was observed by the fluorescence microscope.

## Detection of Mitochondrial Membrane Potential

The mitochondrial membrane potential ( $\Delta\Psi_m$ ) of HepG2 cells was detected by loading 5,5',6,6'-Tetrachloro-1,1',3,3'-tetraethyl-imidacarbocyanine iodide (JC-1) fluorescence probe to assay the early apoptotic cells. According to the directions of the specification sheet,  $1 \times 10^5$  HepG2 cells were cultured per well in 24-well-microplates for the night. About 6 h after treatment, each well was washed twice with fresh PBS. Adding JC-1 fluorescence probe with the amount of 2  $\mu$ L in each well and incubating for 20 min at 37 °C without light. After washing twice with PBS, and adding fresh DMEM, we could observe fluorescence through a fluorescence microscope. When the change of  $\Delta\Psi_m$  appeared, the JC-1 aggregate (red) would trans into the monomer (green), and we could observe it through fluorescence microscope. It means that the mitochondrial membrane of HepG2 cells was damaged and early apoptosis occurred.

## Cell Apoptosis Assay

Following the guidance, cell apoptosis was checked with the Annexin V-AbFluor™ 488/PI Apoptosis Detection kit (Abbkine Inc., Wuhan, China).  $5 \times 10^5$  HepG2 cells per well were seeded into 6-well-microplates and suffered from different treatments overnight. And then, collected approximately  $1 \times 10^5$  HepG2 cells which were assimilated. Washed cells with PBS at 4 °C three times, and resuspended in 100  $\mu$ L of 1 $\times$ binding buffer. 5  $\mu$ L Annexin V-AbFluor™ 488 and 2  $\mu$ L Propidium Iodide (PI) were added to the cell suspension and protected from light for 15 min. After that, 400  $\mu$ L of



1×binding buffer was added in simple, mixed adequately on ice, and detected by flow cytometry (Attune NxT, Thermo Fisher Scientific, USA) within 30min. Therefore, apoptotic cells were stained with Annexin V-AbFluor™ 488<sup>+</sup>/PI<sup>-</sup> (early apoptotic cells) and Annexin V-AbFluor™ 488<sup>+</sup>/PI<sup>+</sup> (late apoptotic cells).

## Cell Autophagy Assay

We cultured  $5 \times 10^4$  HepG2 cells per well in 24-well-microplates for 24 h. Then, 30  $\mu$ L adenovirus expressing mCherry-GFP-LC3B fusion protein (Ad-mCherry-GFP-LC3B, Beyotime Institute of Biotechnology, Jiangsu, China) was mixed with 470  $\mu$ L DMEM, added to every well and train at 37 °C for 24 h. After 24 h of treatment, autophagy in HepG2 cells was observed through the fluorescence microscope. After HepG2 cells were infected by adenovirus, the fusion proteins of mCherry, GFP, and LC3B were effectively expressed in target cells, showing bright red fluorescence and green fluorescence. When autophagy occurs, autophagosomes combine with lysosomes to form autolysosomes. The acidic environment of lysosome would lead to the quenching of GFP fluorescence, while mCherry fluorescence could be retained because of its stability. Therefore, the cells without autophagy would show yellow fluorescence, and the cells that have autophagy would show red fluorescence.

## Cell Scratch Assay

$5 \times 10^4$  HepG2 cells were cultured in each well of 6-well-microplates for 24 h. After different treatments, used a 10  $\mu$ L pipette tip to draw three straight lines in each hole, and took pictures in the same position at 0 h, 24 h, and 48h by electron microscope. The area of scratches was measured by ImageJ software (National Institutes of Health, Bethesda, MD, USA). By comparing the scratch area at different time points, the migration ability and relative migration rate of HepG2 cells after therapy were assayed.

## Transwell Assay

Cell invasion ability was tested using transwell plates (Costar, USA) containing chamber inserts with pore sizes of 8.0  $\mu$ m. First of all, spread 20  $\mu$ L of Matrix-Gel™ Basement Membrane Matrix (Extracellular Matrix, ECM, Beyotime Institute of Biotechnology, Jiangsu, China) on the upper chamber. Approximately  $5 \times 10^4$  cells with different treatments were seeded in the upper chamber in 200  $\mu$ L of the serum-free medium. Later, about 1000  $\mu$ L medium containing 10% FBS in the lower chamber was used to induce cell invasion. After 24 h of incubation, the HepG2 cells on the lower membrane surface were fixed with 10% methanol solution (Beyotime Institute of Biotechnology, Jiangsu, China) for 30 min and stained for 30 min with 0.5% crystal violet solution (Beyotime Institute of Biotechnology, Jiangsu, China). After carefully washing with PBS twice, wiping off the cells and ECM in the upper chamber, and quantifying the invasive cells in the lower chamber by electron microscope.

## Statistical Analysis

The GraphPad Prism 9.5.0 software (San Diego, CA, USA) was used for statistical analysis. All data were presented as mean  $\pm$  standard deviation, and the level of statistical significance was set at  $p < 0.05$ . Student's *t*-test was used to evaluate the statistical difference between the two groups, and a one-way analysis of variance was conducted to compare multiple groups.

## Results

### Fabrication and Characterization of IR-820@NBs

Compared with NBs, IR-820@NBs showed uniformly light gray in appearance. We could observe that IR-820@NBs are spherical and uniformly distributed in an aqueous solution by TME (Figure 1B and C). The results of the DLS measurement showed that the particle size of IR-820NBS is  $108.7 \pm 26.4$  nm, which was consistent with the results of TEM (Figure 1D). The zeta potential analysis of IR-820@NBS showed that the carrier IR-820 did not change the potential level of NBS (Figure 1E). To explore its stability, the particle size of IR-820@NBs did not change obviously when it was placed at room temperature 24H. To confirm that IR-820 was successfully installed in NBs, we recorded the

absorption spectra of IR-820, IR-820@NBs, and pure NBs, and made their concentration absorption intensity curves by recording the absorption spectra of different concentrations of IR-820. As could be seen in Figure 1F, the characteristic absorption peaks of IR-820 and IR-820@NBs were similar, indicating the successful preparation of IR-820@NBs. According to the concentration absorption intensity curve, the drug entrapment efficiency of IR-820@NBs can be calculated to be 75.74% (Figure 1G).

## Intracellular ROS Generation

As shown in Figures 2A and B, only weak fluorescence was detected in the group treated with MG-132 alone, indicating that MG-132 did not damage HepG2 cells by inducing ROS. Compared with the control group, the IR-820+MG-132 treatment group, and the IR-820@NBs+MG-132 treatment group, the IR-820+US treatment group could detect a certain amount of green fluorescence. This shows that IR-820 as a sonosensitizer could hardly induce intracellular ROS production without US irradiation, but could mediate intracellular ROS production and cell damage under US irradiation.

A large number of strong green fluorescence observed in the IR-820@NBs+MG-132+US treatment group showed that combined treatment could better induce the production of ROS. Compared with other experimental groups, on the one hand, it might be due to the UTND effect, the cavitation effect produced by NBs blasting changes the cell membrane permeability, and HepG2 cells could absorb more drugs. Due to the existence of the sonoluminescence effect and sonofever effect, the IR-820@NBs had a stronger ability to induce ROS production. On the other hand, MG-132 could promote apoptosis and autophagy, which might also promote the induction of ROS in the process of SDT.

## Mitochondrial Membrane Depolarization in SDT

The process of SDT treatment mainly depends on the production of intracellular ROS induced by US irradiation. The accumulation of a large amount of ROS in cells would cause damage to mitochondria first. And then, cell damage was induced through the mitochondrial-apoptosis pathway. The change of  $\Delta\Psi_m$  was one of the earliest intracellular changes when apoptosis occurred. To confirm that apoptosis during treatment was caused by SDT, we used JC-1 probes to load cells. When the  $\Delta\Psi_m$  kept at a high level, JC-1 existed in the mitochondrial matrix in the form of aggregates, showing red fluorescence. However, when the  $\Delta\Psi_m$  decreased, JC-1 could no longer gather in the matrix and transform into monomers, showing green fluorescence.

The change could be directly observed by the fluorescence microscope. As shown in Figure 3, compared with other experimental groups, we could only observe this change in the IR-820+US group and the IR-820@NBs+MG-132+US group. This indicated that apoptosis occurred in HepG2 cells during the treatment of SDT. And IR-820@NBs+MG-132+US treatment group showed stronger fluorescence, which proved that combined therapy could increase the level of apoptosis in the process of SDT.

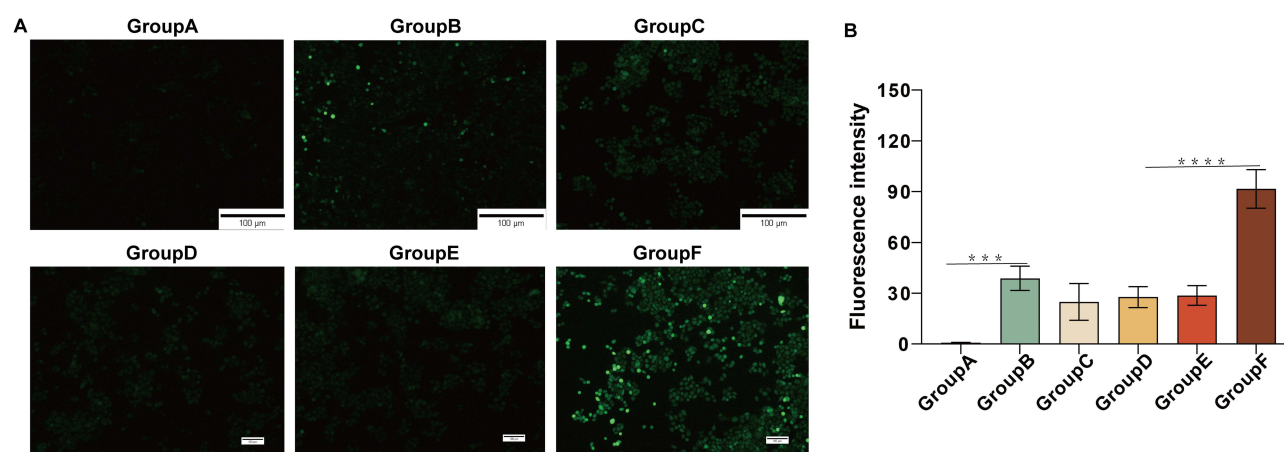


**Figure 2** ROS generation effect of different treat in HepG2 cells. (A) Detection of intracellular ROS generation. (B) Statistical analysis of fluorescence intensity in different experimental groups.\*\*\* $p < 0.001$ , \*\*\*\* $p < 0.0001$ .

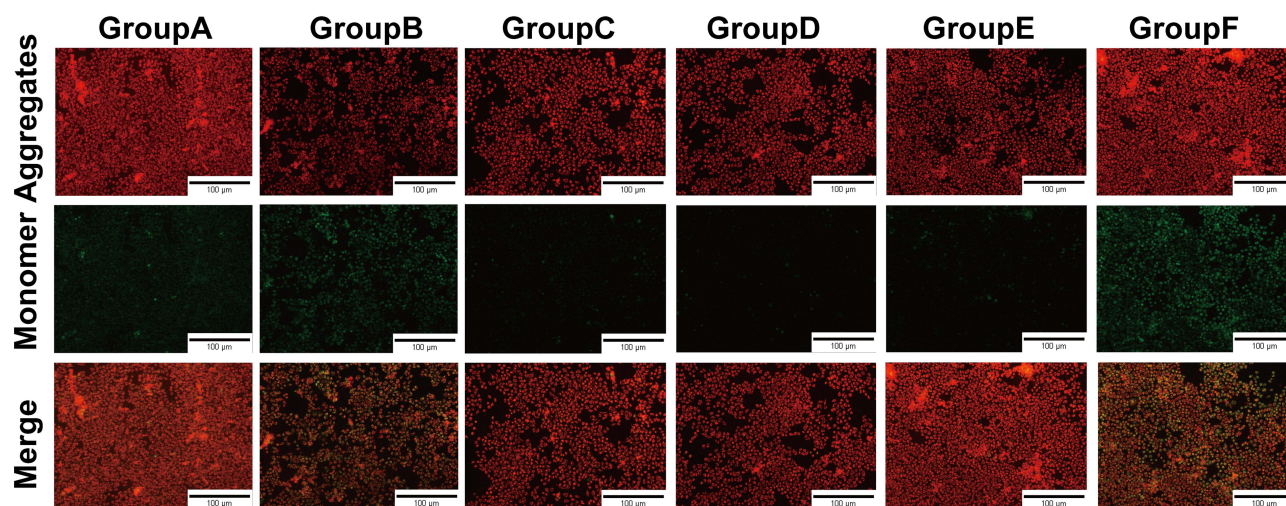


**Figure 3** Involvement of mitochondrial membrane depolarization in combination treatment induced apoptosis.

## Synergistic Cytotoxicity of MG-132 and SDT to HepG2 Cells

To evaluate the cytotoxicity of IR-820 and MG-132, the standard CCK-8 assay was used to determine the survival rate of HepG2 cells after co-incubation with IR-820 (concentration: 0.01–8  $\mu\text{M}$ ) without US irradiation and MG-132 (concentration: 0.1–9  $\mu\text{M}$ ) for 24 h. As shown in [Figure 4A](#), MG-132 could inhibit the cell activity of HepG2 cells in a dose-dependent manner, and its half maximum inhibitory concentration ( $\text{IC}_{50}$ ) was 3.009  $\mu\text{M}$ . Similarly, the  $\text{IC}_{50}$  of IR-820 without US irradiation for HepG2 cells was 2.593  $\mu\text{M}$  ([Figure 4B](#)). To improve the therapeutic effect of SDT and reduce the side effects of drugs on normal cells, the relatively less cytotoxic concentration of IR-820 was selected and different US power density was used to screen the best treatment conditions of SDT ([Figure 4C](#)). We could find that when the concentration of IR-820 was 1  $\mu\text{M}$  and the intensity of US was 3  $\text{W}/\text{cm}^2$ , SDT treatment independently could achieve half inhibitory effect on HepG2 cells. At same the time, the drug side effects and US treatment had less effect on normal cells in this condition.

In addition, according to the experimental results, carrying IR-820 in NBs would not affect the effectiveness of the drug in normal circumstances. Due to the construction of IR-820@NBs, IR-820 could overcome its poor water solubility and scattered distribution in vivo. To further explore the synergistic effect of MG-132 and SDT, we selected a safer concentration of MG-132 and SDT to treat HepG2 cells. As shown in [Figure 4D](#), the cell activity after combined therapy was only  $22.2 \pm 1.3\%$ , indicating that MG-132 could effectively cooperate with SDT in anti-tumor therapy.

## MG-132 Enhancement of SDT-Induced Cell Apoptosis

To explore the relationship between the decrease of HepG2 cells activity and apoptosis, double staining with Annexin V and PI was used after treatment for 24 h, and then the apoptosis was quantitatively analyzed by flow cytometry. According to the experimental results, we found that both SDT and MG-132 could damage HepG2 cells by inducing apoptosis. Moreover, compared with the IR-820+MG-132 treatment group and the IR-820@NBs+MG132 treatment group, the addition of NBs did not change the ability of IR-820 to induce apoptosis. Compared with other treatment groups, the level of apoptosis increased significantly up to  $82.6 \pm 2.6\%$  when treated with MG-132 and SDT ([Figure 4E](#) and [F](#)). This shows that MG-132 could effectively improve the level of apoptosis induced by SDT, reflecting the advantages of combined therapy.

## Cell Autophagy Induced by MG-132 and SDT

LC3B was a subfamily of microtubule-associated protein 1 light chain 3 (MAP1LC3) and it could be a marker protein in the process of autophagy. Different from LC3B I, which was located in the cytoplasm, LC3B II was located on the intima



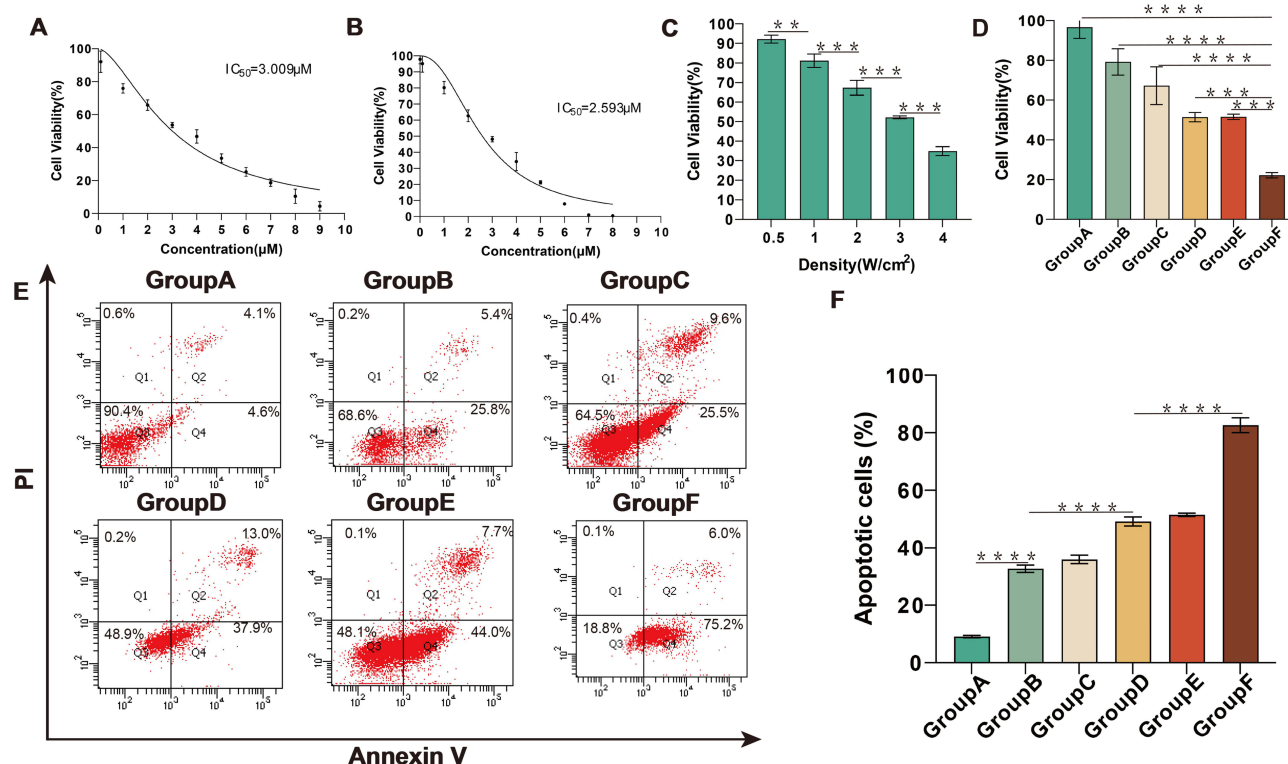


**Figure 4** Therapy effect of different treat in HepG2 cells. **(A)** HepG2 cells were treated with MG-132 (concentration: 0.1–9 μM) for 24 h, and the cell survival rate was detected by CCK-8 assay. **(B)** HepG2 cells were treated with IR-820 (concentration: 0.01–8 μM) for 24 h, and the cell survival rate was detected by CCK-8 assay. **(C)** HepG2 cells were irradiated with different US power density, and the cell survival rate was detected by CCK-8 assay. **(D)** HepG2 cells were treated with different treatment, and the cell survival rate was detected by CCK-8 assay. **(E)** HepG2 cells were treated with different treatment for 24 h, and then stained with Annexin-V and PI before being analyzed by flow cytometry. **(F)** Statistical results from different experiments of cell apoptosis in HepG2 cells. \*\* $p < 0.01$ , \*\*\* $p < 0.001$ , \*\*\*\* $p < 0.0001$ .

and adventitia of autophagosomes. When the autophagosome binds to the lysosome, the LC3B II on the autophagosome was swallowed by the lysosome.<sup>29</sup> Ad-mCherry-GFP-LC3B could be used to mark LC3B specifically. When autophagy occurred in HepG2 cells, autolysosomes were formed and mCherry-GFP-LC3B was swallowed by lysosomes. At this time, GFP would be quenched by the acidic environment of the lysosome, therefore, the autophagy cells could only see red fluorescence in the fluorescence microscope.

Except for yellow fluorescence in the control group, all the other experimental groups showed partial yellow fluorescence and partial red fluorescence (Figure 5A). This shows that SDT independently could not only induce apoptosis but also induce autophagy. And the level of autophagy would increase during the combined treatment of MG-132 and SDT. In addition, we found that the fluorescence intensity and virus transfection efficiency of the control group were lower than those of other experimental groups, which might be due to the existence of treatment methods to improve the adenovirus transfection rate. In a word, autophagy existed in the process of SDT therapy, and combined therapy could improve the level of autophagy in the process of treatment.

## Synergistic Anti-Tumor Effect of Apoptosis and Autophagy

To verify the relationship between apoptosis and autophagy induced during treatment, chloroquine (Cq), one kind of autophagy inhibitor, was used to inhibit autophagy during treatment. As shown by the CCK-8 assay results, when autophagy was inhibited, the cell activity of the treatment group increased from  $30.23 \pm 0.04\%$  to  $42.87 \pm 0.02\%$  (Figure 5B). This shows that autophagy produced in the process of combined therapy had a damaging effect on cells. Interestingly, the results of flow cytometry showed that the apoptosis rate of HepG2 cells decreased by  $13.80 \pm 1.99\%$  when autophagy was inhibited (Figure 5C and D). The experimental result shows that autophagy and apoptosis promote HepG2 cells death in the process of combined therapy. When autophagy was inhibited, the level of apoptosis decreased.

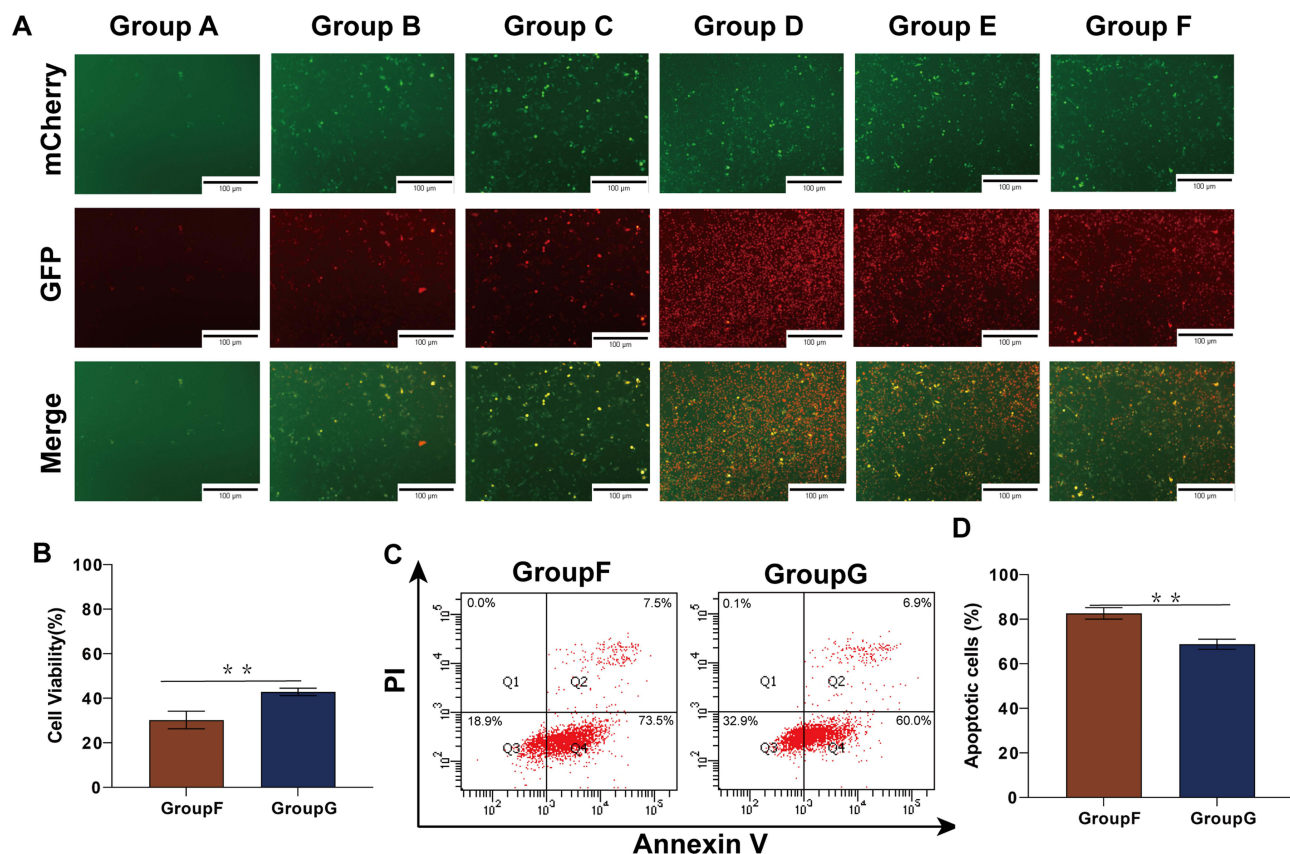


**Figure 5** Autophagy were induced in the treatment process, and explore the relationship between autophagy and apoptosis by inhibiting autophagy. **(A)** HepG2 cells were transfected using Ad-mCherry-GFP-LC3B, and the occurrence of autophagy was visualized by fluorescence microscopy. **(B)** Changes of HepG2 cell activity after inhibition of autophagy by chloroquine, and the cell survival rate was detected by CCK-8 assay. **(C)** HepG2 cells were treated with combined therapy and inhibiting autophagy before treatment, and then stained with Annexin-V and PI before being analyzed by flow cytometry. **(D)** Statistical results of cell apoptosis in HepG2 cells after inhibiting autophagy. \*\* $p < 0.01$ .

This suggested that part of the apoptosis induced by SDT may be transformed from autophagy. All in all, in the process of combined therapy, autophagy can cooperate with apoptosis to achieve the anti-tumor effect.

## Suppression of HepG2 Migration and Invasion Ability

Cell migration ability and cell invasion ability were the basic abilities of tumor cells. Here, we evaluated the migration and invasion ability of HepG2 cells by cell scratch assay and transwell assay. As shown in the figure, compared with other experimental groups, the healing rates of scratched areas in the MG-132 and SDT combined treatment groups were  $4.8 \pm 1.8\%$  and  $10.6 \pm 1.4\%$  at 24 h and 48 h, respectively (Figure 6A–C). According to the results of the transwell assay, the number of HepG2 across the membrane in the combined treatment group decreased significantly, indicating that the invasive ability of tumor cells decreased significantly (Figure 7A and B). Therefore, it could be concluded that combination therapy could inhibit the migration and invasion of HepG2 cells effectively.

## Discussion

Although there are many basic research and clinical trials for the treatment of liver cancer, the current clinical treatment methods have some problems, such as large trauma, low long-term survival rate, large drug side effects, chemotherapy resistance, and so on.<sup>3,30</sup> Therefore, it is important to develop a safer treatment as adjuvant therapy or even an alternative therapy for liver cancer. SDT gradually appears in the field of tumor treatment research because of its advantages such as non-invasive and strong safety.<sup>31</sup> Present studies have shown that SDT alone or in combination with other antineoplastic



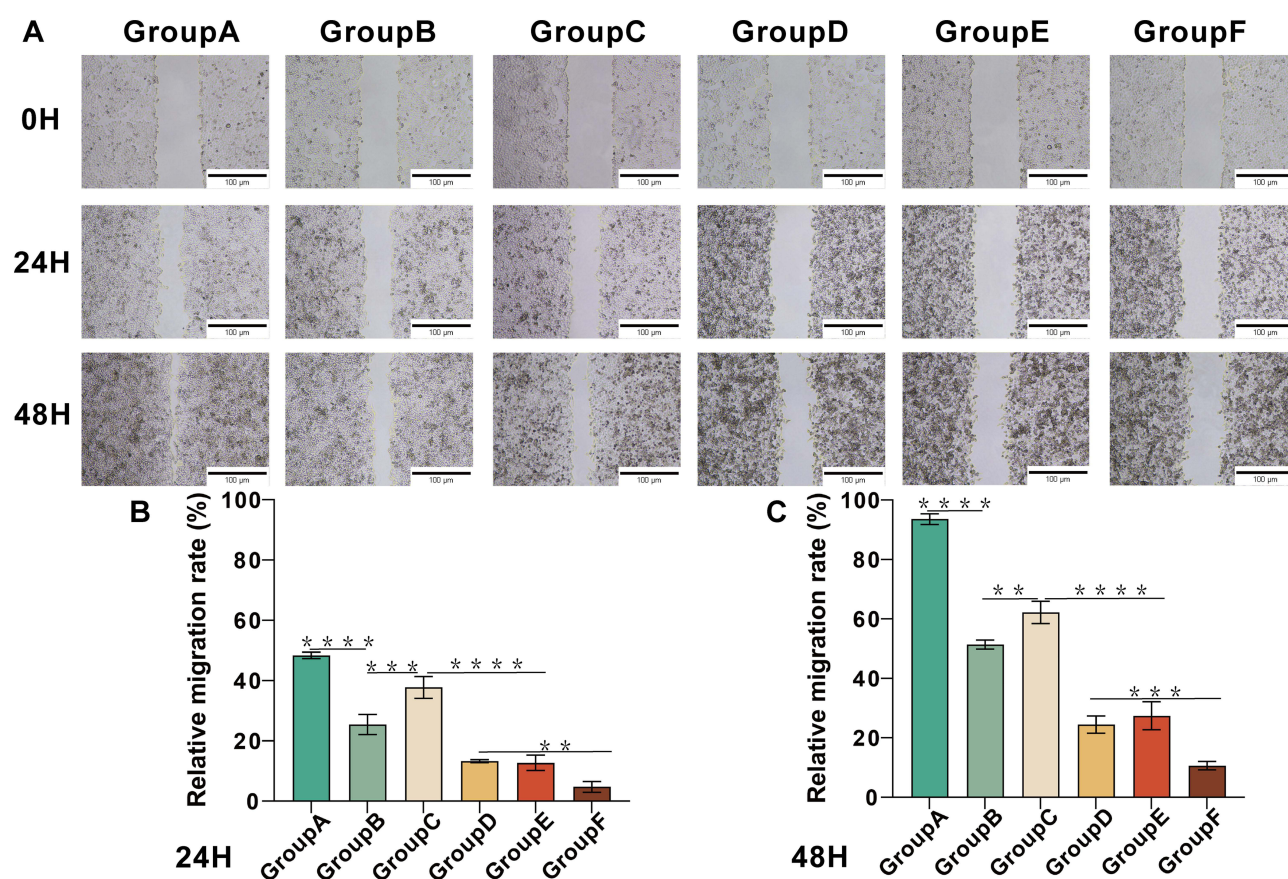


**Figure 6** Combination therapy reduced the migration ability of HepG2 cells. **(A)** Scratch assay of HepG2 cells at 24 h and 48 h after different treatment. **(B and C)** Statistical results of relative migration rate of HepG2 cells at 24 h and 48 h after different treatments. \*\* $p < 0.01$ , \*\*\* $p < 0.001$ , \*\*\*\* $p < 0.0001$ .

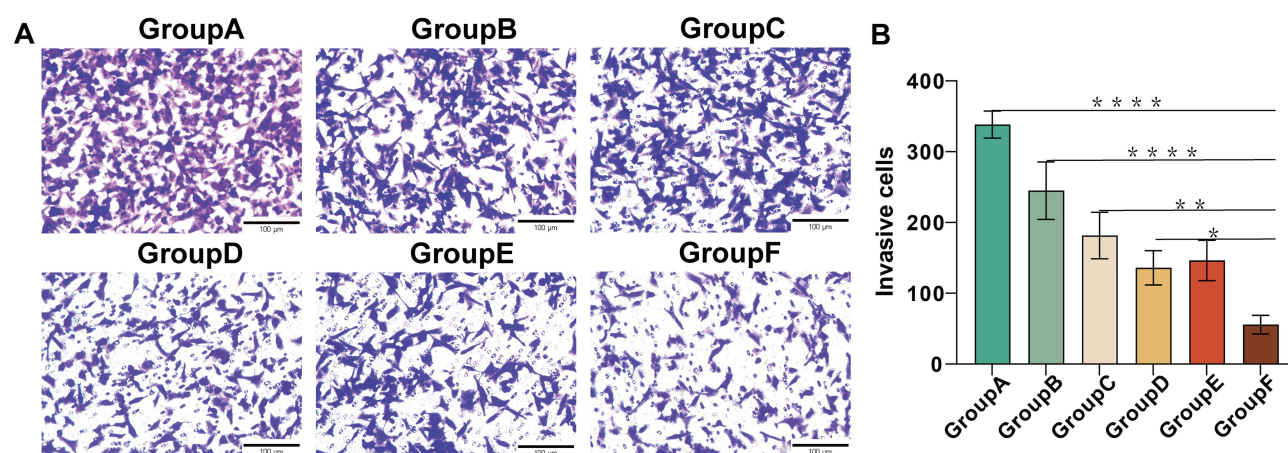


**Figure 7** Combination therapy reduced the invasion ability of HepG2 cells. **(A)** Transwell assay was performed in HepG2 cells to investigate the inhibitory effect of combination treatment on HCC metastatic processes. **(B)** Quantitation of migrated cell number of HepG2 cells. \* $p < 0.05$ , \*\* $p < 0.01$ , \*\*\*\* $p < 0.0001$ .

drugs could effectively treat liver cancer.<sup>32</sup> However, the poor stability and low biocompatibility of traditional sonosensitizers limit the therapeutic effect of SDT and the opportunity for clinical application in the future.

Due to the EPR effect, nanoparticles carrying therapeutic drugs play an important role in the anti-tumor therapy of nanomedicine.<sup>33</sup> Among them, NBs were widely used because of their positive biosafety and other advantages.<sup>34</sup> In this study, we successfully prepared spherical IR-820@NBs with uniform particle size and the average particle size was 108.7

$\pm 26.4$  nm. According to the previous research results, using NBs to carry sonosensitizer could not only passively target tumor cells through the EPR effect, but also achieve targeted drug release and improve the drug uptake rate of tumor cells through UTND technology, to improve the therapeutic effect of SDT.<sup>35</sup> The IR-820@NBs could overcome the shortcomings of IR-820 such as strong hydrophobicity, to better mediate SDT in the treatment of HCC.

SDT mainly achieves tumor therapy based on inducing ROS production in tumor cells with the sonosensitizer irradiated by US. As the organelle of cellular respiration, mitochondria were easily affected by ROS accumulation. The increase of ROS level would lead to lipid peroxidation of the mitochondrial membrane and cell membrane, which would cause cell death by intrinsic and extrinsic apoptosis signal pathways.<sup>36</sup> On the one hand, the damage to the mitochondrial membrane (mitochondrial stress) would lead to the release of Cyt C in mitochondria, which leads to the activation of the caspase family signals pathway and induces tumor cell apoptosis.<sup>37</sup> On the other hand, lipid peroxidation could up-regulate apoptosis through endoplasmic reticulum stress (ER stress) and induce apoptosis through TRAIL and FAS pathways.<sup>38,39</sup> Therefore, the ability to induce the production of ROS could be used as one of the indexes to judge the effectiveness of the sonosensitizer. In this work, we found that SDT mediated by IR-820@NBs could effectively induce the production of ROS and the change of mitochondrial membrane potential. Indicating that SDT could effectively induce apoptosis of HCC cells, and the results of flow cytometry and CCK-8 could also explain this result.

Autophagy refers to the process of cytoplasmic material transport to lysosome degradation, including macroautophagy, microautophagy, and molecular chaperone-mediated autophagy.<sup>40</sup> ROS could mediate autophagy through ER stress-activated PKR-like ER kinase (PERK) pathway due to lipid peroxidation, accompanied by c-JunN-terminal kinase (JNK) activation.<sup>41,42</sup> Hydroxynonenal (HNE), as a product of lipid peroxidation, could also activate autophagy by regulating mitogen-activated protein kinase (MAPK)-mammalian target of rapamycin (mTOR), phosphoinositol 3-kinase (PI3K)-AKT-mTOR and protein kinase C (PKC) pathways.<sup>43</sup> In addition, ROS could induce autophagy directly by activating (AMP)-activated protein kinase (AMPK) which would activate autophagy protein ULK1 directly or inhibit the mTOR pathway.<sup>44</sup> Therefore, autophagy could be induced during the treatment of SDT, and the occurrence of autophagy was confirmed by the detection of mCherry-GFP-LC3B.

Tumor suppressor gene p53 could regulate the cell cycle and induce apoptosis, which plays an important role in the growth of HCC cells.<sup>45</sup> The degradation of p53 pro-apoptotic protein was mainly through UPS, so the inhibition of UPS was helpful in restoring the activity of the p53 protein.<sup>26</sup> Previous studies have shown that tumor cells treated with MG-132 could up-regulate the p53 protein in tumor cells, thus promoting the activation of caspase-8 and inducing cell apoptosis. P53 localized in the cytoplasm could inhibit autophagy. After MG-132 treatment, the restored activity of p53 changed from cytoplasmic to nuclear. This p53 localized in the nucleus was directly related to the activation of autophagy.<sup>28,46</sup> While up-regulating pro-apoptotic proteins, MG-132 could also down-regulate the expression of anti-apoptotic proteins such as Bcl-2, thus acting as a dual agonist of apoptosis and autophagy.<sup>47</sup> In our study, compared with other experimental groups, the apoptosis rate and autophagy fluorescence intensity of HepG2 cells treated with SDT combined with MG-132 were the highest. MG-132 could effectively improve the therapeutic effect of SDT.

Due to many components being identical in the pathway of apoptosis and autophagy, the relationship between apoptosis and autophagy is complicated. At a certain level of stress, autophagy could inhibit apoptosis by selectively reducing the abundance of pro-apoptotic proteins.<sup>48</sup> But excessive autophagy could also promote apoptosis. A large number of autophagy proteins could induce apoptosis, and autophagy would also promote apoptosis by degrading anti-apoptotic factors and changing the open state of the mitochondrial membrane.<sup>49,50</sup> Similarly, apoptosis could also promote or inhibit autophagy through apoptosis signals and apoptosis products.<sup>51</sup> Therefore, it is necessary to verify the relationship between apoptosis and autophagy during SDT treatment. After using Cq to inhibit the occurrence of autophagy, we were surprised to find that the cell activity of the Cq-treated group was improved, and the results of flow cytometry showed that the apoptosis rate of the Cq-treated group decreased. Apoptosis and autophagy were regulated by Bcl2 and AMBAR1, both of which exist in mitochondria and endoplasmic reticulum. Regardless of the stress state of the endoplasmic reticulum, apoptosis was only sensitive to mitochondrial stress. When the mitochondria were in a low-stress state, autophagy was induced but no apoptosis existed. When the mitochondria are in a state of high stress, autophagy and apoptosis both were induced by Bcl2. Due to the increase of caspase activity and the inactivation of Beclin1-A, autophagy gradually converts to apoptosis.<sup>52</sup> When autophagy inhibitors were used, the decrease of apoptotic cells

indicates that apoptosis has a certain degree of autophagy dependence.<sup>22</sup> Therefore, we speculated that in the process of combined therapy of HCC, the mitochondria of HepG2 cells were in a state of high stress because a large amount of ROS was induced. The addition of MG-132 aggravated the stress state of mitochondria, promoted the transformation of autophagy into apoptosis, and induced autophagy-dependent apoptosis. In short, SDT combined with MG-132 realized the synergistic anti-tumor therapy of autophagy combined with apoptosis, which originated from autophagy-dependent apoptosis.

The change of migration and invasion ability of tumor cells is another index to evaluate the therapeutic effect of tumors. Previous studies have found that MG-132 could inhibit the invasion and migration of tumor cells by promoting the expression of E-cadherin and up-regulating E26 transformation-specific family transcription factor (ESE3).<sup>53</sup> Therefore, we used cell scratch assay and transwell assay to detect the migration and invasion ability of HepG2 cells treated with SDT combined with MG-132. The results showed that the migration and invasion ability of HepG2 cells decreased significantly after combined therapy. MG-132 could enhance the therapeutic effect of SDT on HCC cells, induce its death, and inhibit its invasion and metastasis at the same time.

In this study, we confirmed that MG-132 combined with SDT could effectively treat HCC. As a dual agonist of apoptosis and autophagy, MG-132 could effectively improve the therapeutic effect of SDT. However, there are still some limitations in this experiment. First of all, the target of this study is only the HepG2 cell line, but the effect on other HCC cell lines is not deep. Secondly, although the experimental results show that combined therapy could mediate apoptosis and autophagy in anti-tumor therapy, its potential mechanism has not been explored. Finally, this experiment is only verified in vitro, but not in vivo. These will be the direction of the following research.

## Conclusion

The experimental results of this study proved that IR-820@NBs-mediated SDT combined with MG-132 could effectively promote HCC cell apoptosis and autophagy, and inhibit tumor growth and metastasis, thus showing a good anti-tumor effect. MG-132 can effectively promote the occurrence of autophagy and apoptosis during SDT. Combination therapy is mainly based on the induction of ROS production at lethal levels within HepG2 cells. The pretreatment results of autophagy inhibitors showed that the part apoptosis of HepG2 cells was transformed from autophagy. Our results propose a new point to the relationship between autophagy and apoptosis, that is, to promote apoptosis through over-induction of autophagy, and bring new ideas to solve problems such as chemotherapy resistance. On the other hand, our findings will contribute to the development of non-invasive tumor therapy in the future and bring new options for the clinical treatment of cancer.

## Acknowledgments

The experimental site was provided by Cancer Research affiliated with Harbin Medical University.

## Funding

The research was supported by the National Natural Science Foundation of China (grant numbers 82171947 and 82202163) and Key Project of Provincial Natural Science Foundation (grant numbers ZD2021H005).

## Disclosure

The authors report no conflicts of interest in this work.

## References

1. Elewa MAF, Eldehna WM, Hamdan AME, et al. WRH-2412 alleviates the progression of hepatocellular carcinoma through regulation of TGF-beta/beta-catenin/alpha-SMA pathway. *J Enzyme Inhib Med Chem*. 2023;38(1):2185761. doi:10.1080/14756366.2023.2185761
2. Villanueva A, Lango DL. Hepatocellular Carcinoma. *N Engl J Med*. 2019;380(15):1450–1462. doi:10.1056/NEJMr1713263
3. Siegel RL, Miller KD, Jemal A. Cancer statistics, 2018. *CA Cancer J Clin*. 2018;68(1):7–30. doi:10.3322/caac.21442
4. Lai Y, Lu N, Ouyang A, Zhang Q, Zhang P. Ferroptosis promotes sonodynamic therapy: a platinum(ii)-indocyanine sonosensitizer. *Chem Sci*. 2022;13(34):9921–9926. doi:10.1039/d2sc02597c



5. Zhang L, Zhu P, Wan T, Wang H, Mao Z. Glutamine coated titanium for synergistic sonodynamic and photothermal on tumor therapy upon targeted delivery. *Front Bioeng Biotechnol.* **2023**;11:1139426. doi:10.3389/fbioe.2023.1139426
6. Wang Z, Yu N, Zhang J, Ren Q, Li M, Chen Z. Nanoscale Hf-hematoporphyrin frameworks for synergetic sonodynamic/radiation therapy of deep-seated tumors. *J Colloid Interface Sci.* **2022**;626:803–814. doi:10.1016/j.jcis.2022.06.174
7. Zheng X, Liu W, Ge J, et al. Biodegradable natural product-based nanoparticles for near-infrared fluorescence imaging-guided sonodynamic therapy. *ACS Appl Mater Interfaces.* **2019**;11(20):18178–18185. doi:10.1021/acsami.9b03270
8. Hu H, Liu X, Hong J, et al. Mesoporous polydopamine-based multifunctional nanoparticles for enhanced cancer phototherapy. *J Colloid Interface Sci.* **2022**;612:246–260. doi:10.1016/j.jcis.2021.12.172
9. Zhu L, Chen J, Yan T, et al. Near-infrared emissive polymer-coated IR-820 nanoparticles assisted photothermal therapy for cervical cancer cells. *J Biophotonics.* **2021**;14(11):e202100117. doi:10.1002/jbio.202100117
10. Nittayacharn P, Abenojar E, De Leon A, Wegierak D, Exner AA. Increasing doxorubicin loading in lipid-shelled perfluoropropane nanobubbles via a simple deprotonation strategy. *Front Pharmacol.* **2020**;11:644. doi:10.3389/fphar.2020.00644
11. Liu Z, Zhang J, Tian Y, et al. Targeted delivery of reduced graphene oxide nanosheets using multifunctional ultrasound nanobubbles for visualization and enhanced photothermal therapy. *Int J Nanomedicine.* **2018**;13:7859–7872. doi:10.2147/IJN.S181268
12. Lan M, Zhu L, Wang Y, et al. Multifunctional nanobubbles carrying indocyanine green and paclitaxel for molecular imaging and the treatment of prostate cancer. *J Nanobiotechnology.* **2020**;18(1):121. doi:10.1186/s12951-020-00650-1
13. Tower J. Programmed cell death in aging. *Ageing Res Rev.* **2015**;23(Pt A):90–100. doi:10.1016/j.arr.2015.04.002
14. Rongvaux A, Jackson R, Harman CC, et al. Apoptotic caspases prevent the induction of type I interferons by mitochondrial DNA. *Cell.* **2014**;159(7):1563–1577. doi:10.1016/j.cell.2014.11.037
15. Li P, Gong X, Yuan L, et al. Palmitoylation in apoptosis. *J Cell Physiol.* **2023**. doi:10.1002/jcp.31047
16. Zhou T, Mo J, Xu W, et al. Mild hypothermia alleviates oxygen-glucose deprivation/reperfusion-induced apoptosis by inhibiting ROS generation, improving mitochondrial dysfunction and regulating DNA damage repair pathway in PC12 cells. *Apoptosis.* **2023**;28(3–4):447–457. doi:10.1007/s10495-022-01799-w
17. Basu A. The interplay between apoptosis and cellular senescence: bcl-2 family proteins as targets for cancer therapy. *Pharmacol Ther.* **2022**;230:107943. doi:10.1016/j.pharmthera.2021.107943
18. Ikeda S, Zablocki D, Sadoshima J. The role of autophagy in death of cardiomyocytes. *J Mol Cell Cardiol.* **2022**;165:1–8. doi:10.1016/j.yjmcc.2021.12.006
19. Yang J, Sun Y, Xu F, et al. Autophagy and glycolysis independently attenuate silibinin-induced apoptosis in human hepatocarcinoma HepG2 and Hep3B cells. *Hum Exp Toxicol.* **2021**;40(12):2048–2062. doi:10.1177/09603271211017609
20. Tang ZN, Bi XF, Chen WL, Zhang CL. RANKL promotes chemotherapy resistance in breast cancer cells through STAT3 mediated autophagy induction. *Clin Breast Cancer.* **2023**;23(4):388–396. doi:10.1016/j.clbc.2023.01.014
21. Dong Y, Jin Q, Sun M, et al. CLDN6 inhibits breast cancer metastasis through WIP-dependent actin cytoskeleton-mediated autophagy. *J Exp Clin Cancer Res.* **2023**;42(1):68. doi:10.1186/s13046-023-02644-x
22. Cao C, Huang W, Zhang N, et al. Narciclasine induces autophagy-dependent apoptosis in triple-negative breast cancer cells by regulating the AMPK-ULK1 axis. *Cell Prolif.* **2018**;51(6):e12518. doi:10.1111/cpr.12518
23. Chen F, Cai X, Kang R, Liu J, Tang D. Autophagy-dependent ferroptosis in cancer. *Antioxid Redox Signal.* **2023**;39(1–3):79–101. doi:10.1089/ars.2022.0202
24. Su X, Wang P, Yang S, Zhang K, Liu Q, Wang X. Sonodynamic therapy induces the interplay between apoptosis and autophagy in K562 cells through ROS. *Int J Biochem Cell Biol.* **2015**;60:82–92. doi:10.1016/j.biocel.2014.12.023
25. Li Y, Li S, Wu H. Ubiquitination-Proteasome System (UPS) and autophagy two main protein degradation machineries in response to cell stress. *Cells.* **2022**;11(5). doi:10.3390/cells11050851
26. Zhang W, Xu W, Chen W, Zhou Q. Interplay of autophagy inducer rapamycin and proteasome inhibitor MG132 in reduction of foam cell formation and inflammatory cytokine expression. *Cell Transplant.* **2018**;27(8):1235–1248. doi:10.1177/0963689718786229
27. Bu Z, Yang J, Zhang Y, et al. Sequential ubiquitination and phosphorylation epigenetics reshaping by MG132-loaded Fe-MOF disarms treatment resistance to repulse metastatic colorectal cancer. *Adv Sci.* **2023**;10(23):e2301638. doi:10.1002/adv.202301638
28. Lagunas-Martinez A, Garcia-Villa E, Arellano-Gaytan M, et al. MG132 plus apoptosis antigen-1 (APO-1) antibody cooperate to restore p53 activity inducing autophagy and p53-dependent apoptosis in HPV16 E6-expressing keratinocytes. *Apoptosis.* **2017**;22(1):27–40. doi:10.1007/s10495-016-1299-1
29. Tedesco B, Vendredy L, Timmerman V, Poletti A. The chaperone-assisted selective autophagy complex dynamics and dysfunctions. *Autophagy.* **2023**;19(6):1619–1641. doi:10.1080/15548627.2022.2160564
30. Lv YF, Deng ZQ, Bi QC, et al. Intratumoral Pi deprivation benefits chemoembolization therapy via increased accumulation of intracellular doxorubicin. *Drug Deliv.* **2022**;29(1):1743–1753. doi:10.1080/10717544.2022.2081384
31. Wen M, Zhao Y, Qiu P, et al. Efficient sonodynamic ablation of deep-seated tumors via cancer-cell-membrane camouflaged biocompatible nanosonosensitizers. *J Colloid Interface Sci.* **2023**;644:388–396. doi:10.1016/j.jcis.2023.04.088
32. Li S, Zhang Y, Liu X, et al. Smart NIR-II croconaine dye-peptide for enhanced photo-sonotheranostics of hepatocellular carcinoma. *Theranostics.* **2022**;12(1):76–86. doi:10.7150/thno.64759
33. Chizenga EP, Abrahamse H. Design and assembly of a nanoparticle, antibody, phthalocyanine scaffold for intracellular delivery of photosensitizer to human papillomavirus-transformed cancer cells. *Artif Cells Nanomed Biotechnol.* **2023**;51(1):205–216. doi:10.1080/21691401.2023.2199037
34. Ma Y, Li J, Zhao Y, Hu B, Liu Y, Liu C. Nanobubble-mediated co-delivery of Ce6 and miR-195 for synergized sonodynamic and checkpoint blockade combination therapy with elicitation of robust immune response in hepatocellular carcinoma. *Eur J Pharm Biopharm.* **2022**;181:36–48. doi:10.1016/j.ejpb.2022.10.017
35. Peng Y, Zhu L, Wang L, et al. Preparation of nanobubbles modified with a small-molecule CXCR4 antagonist for targeted drug delivery to tumors and enhanced ultrasound molecular imaging. *Int J Nanomedicine.* **2019**;14:9139–9157. doi:10.2147/IJN.S210478
36. Elkin ER, Harris SM, Loch-Carus R. Trichloroethylene metabolite S-(1,2-dichlorovinyl)-L-cysteine induces lipid peroxidation-associated apoptosis via the intrinsic and extrinsic apoptosis pathways in a first-trimester placental cell line. *Toxicol Appl Pharmacol.* **2018**;338:30–42. doi:10.1016/j.taap.2017.11.006

37. Bock FJ, Tait SWG. Mitochondria as multifaceted regulators of cell death. *Nat Rev Mol Cell Biol.* 2020;21(2):85–100. doi:10.1038/s41580-019-0173-8
38. Tsuzuki T, Kambe T, Shibata A, Kawakami Y, Nakagawa K, Miyazawa T. Conjugated EPA activates mutant p53 via lipid peroxidation and induces p53-dependent apoptosis in DLD-1 colorectal adenocarcinoma human cells. *Biochim Biophys Acta.* 2007;1771(1):20–30. doi:10.1016/j.bbali.2006.11.006
39. Jiang N, Huang R, Zhang J, et al. TIMP2 mediates endoplasmic reticulum stress contributing to sepsis-induced acute kidney injury. *FASEB J.* 2022;36(4):e22228.
40. Tilija Pun N, Jang W-J, Jeong C-H. Role of autophagy in regulation of cancer cell death/apoptosis during anti-cancer therapy: focus on autophagy flux blockade. *Arch Pharm Res.* 2020;43(5):475–488. doi:10.1007/s12272-020-01239-w
41. Csala M, Kardon T, Legeza B, et al. On the role of 4-hydroxynonenal in health and disease. *Biochim Biophys Acta.* 2015;1852(5):826–838. doi:10.1016/j.bbadi.2015.01.015
42. Habertz P, Hill BG. Oxidized lipids activate autophagy in a JNK-dependent manner by stimulating the endoplasmic reticulum stress response. *Redox Biol.* 2013;1(1):56–64. doi:10.1016/j.redox.2012.10.003
43. Martinez-Useros J, Garcia-Foncillas J. Obesity and colorectal cancer: molecular features of adipose tissue. *J Transl Med.* 2016;14(1). doi:10.1186/s12967-016-0772-5
44. Kaminsky VO, Zhivotovsky B. Free radicals in cross talk between autophagy and apoptosis. *Antioxid Redox Signal.* 2014;21(1):86–102. doi:10.1089/ars.2013.5746
45. Choudhary HB, Mandlik SK, Mandlik DS. Role of p53 suppression in the pathogenesis of hepatocellular carcinoma. *World J Gastrointest Pathophysiol.* 2023;14(3):46–70. doi:10.4291/wjgp.v14.i3.46
46. Contreras-Ochoa CO, Lopez-Arellano ME, Roblero-Bartolon G, et al. Molecular mechanisms of cell death induced in glioblastoma by experimental and antineoplastic drugs: new and old drugs induce apoptosis in glioblastoma. *Hum Exp Toxicol.* 2020;39(4):464–476. doi:10.1177/0960327119892041
47. Lee HK, Park SH, Nam MJ. Proteasome inhibitor MG132 induces apoptosis in human osteosarcoma U2OS cells. *Hum Exp Toxicol.* 2021;40(11):1985–1997. doi:10.1177/09603271211017972
48. Rubinstein Assaf D, Eisenstein M, Ber Y, Bialik S, Kimchi A. The autophagy protein Atg12 associates with antiapoptotic Bcl-2 family members to promote mitochondrial apoptosis. *Mol Cell.* 2011;44(5):698–709. doi:10.1016/j.molcel.2011.10.014
49. Nezis IP, Shrivage BV, Sagana AP, et al. Autophagic degradation of dBruce controls DNA fragmentation in nurse cells during late Drosophila melanogaster oogenesis. *J Cell Biol.* 2010;190(4):523–531. doi:10.1083/jcb.201002035
50. Gump JM, Staskiewicz L, Morgan MJ, Bamberg A, Riches DWH, Thorburn A. Autophagy variation within a cell population determines cell fate through selective degradation of Fap-1. *Nat Cell Biol.* 2013;16(1):47–54. doi:10.1038/ncb2886
51. Xi H, Wang S, Wang B, et al. The role of interaction between autophagy and apoptosis in tumorigenesis (Review). *Oncol Rep.* 2022;48(6). doi:10.3892/or.2022.8423
52. Yang B, Liu Q, Bi Y. Autophagy and apoptosis are regulated by stress on Bcl2 by AMBRA1 in the endoplasmic reticulum and mitochondria. *Theor Biol Med Model.* 2019;16(1). doi:10.1186/s12976-019-0113-5
53. Jin F, Xiao D, Zhao T, Yu M. Proteasome inhibitor MG132 suppresses pancreatic ductal adenocarcinoma-cell migration by increasing ESE3 expression. *Oncol Lett.* 2020;19(1):858–868. doi:10.3892/ol.2019.11157

## International Journal of Nanomedicine

Dovepress

### Publish your work in this journal

The International Journal of Nanomedicine is an international, peer-reviewed journal focusing on the application of nanotechnology in diagnostics, therapeutics, and drug delivery systems throughout the biomedical field. This journal is indexed on PubMed Central, MedLine, CAS, SciSearch®, Current Contents®/Clinical Medicine, Journal Citation Reports/Science Edition, EMBASE, Scopus and the Elsevier Bibliographic databases. The manuscript management system is completely online and includes a very quick and fair peer-review system, which is all easy to use. Visit <http://www.dovepress.com/testimonials.php> to read real quotes from published authors.

Submit your manuscript here: <https://www.dovepress.com/international-journal-of-nanomedicine-journal>